JOC The Journal of Organic Chemistry

Article

pubs.acs.org/joc

Mechanism of the OH Radical Addition to Adenine from Quantum-Chemistry Determinations of Reaction Paths and Spectroscopic Tracking of the Intermediates

Antonio Francés-Monerris,* Manuela Merchán, and Daniel Roca-Sanjuán*

Instituto de Ciencia Molecular, Universitat de València, P.O. Box 22085, 46071 València, Spain

Supporting Information

ABSTRACT: The OH radical is a well-known mediator in the oxidation of biological structures like DNA. Over the past decades, the precise events taking place after reaction of DNA nucleobases with OH radical have been widely investigated by the scientific community. Thirty years after the proposal of the main routes for the reaction of •OH with adenine (Vieira, A.; Steenken, S. *J. Am. Chem. Soc.* 1990, *112*, 6986−6994), the present work demonstrates that the OH radical addition to C4 position is a minor pathway. Instead, the dehydration process is mediated by the A5OH adduct. Conclusions are based on density functional theory calculations for the ground-state reactivity and highly accurate multiconfigurational computations for the excited states of the radical intermediates. The methodology has been also used to study the mechanism giving rise to the mutagens 8-oxoA and FAPyA. Taking into account the agreement between the experimental data and the theoretical results, it is concluded that addition to the C5 and C8 positions accounts for at least ∼44.5% of the total •OH reaction in water solution. Finally, the current findings suggest that hydrophobicity in the DNA/RNA surroundings facilitates the formation of 8-oxoA and FAPyA.

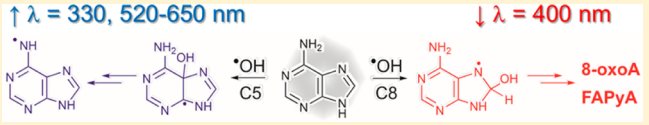

INTRODUCTION

Oxidation of DNA plays a major role in serious diseases like cardiovascular disorders,[1,2] diabetes,[3] retinopathies,[4] cancer,[5] aging,[6] and many others.[7,8] Oxidation is mainly mediated by reactive oxygen species (ROS), a family of highly unstable compounds formed during regular metabolism and by exogenous agents like solar radiation,[9] infections,[10] pollutants,[11] etc. Despite natural defenses against ROS, cellular damage is unavoidable in situations when the balance between damaging and protecting processes is impaired. Among the ROS, the most important species able to modify DNA/RNA nucleobases (NBs) is the OH radical (•OH), which can lead to NB and sugar lesions, strand breaks, and DNA−protein cross-links.[12,13] Even though we now have a good understanding of the enzymatic reparation of DNA/RNA oxidative lesions (see the 2015 Nobel Prize in Chemistry[14]), some aspects of the processes *causing* the damage remain unclear. •OH is able to react rapidly, at almost diffusion-controlled rates, yielding a variety of oxidized products depending on the reaction conditions.[15] All accumulated evidence indicates that OH radical reacts with NBs via three distinct mechanisms, (a) one-electron oxidation, (b) addition to the C5═C6 bond of pyrimidines and the C4═C5 and N7═C8 bonds of purines, and (c) abstraction of H atoms from the NBs and sugar moieties.[15] These processes have been extensively studied in isolated NBs, nucleosides, and nucleotides in solution as model systems[16−21] in order to understand the intrinsic properties of the building blocks, as a previous step in the comprehension of the events in the DNA environment. A correct interpretation of the relatively simple systems is therefore of paramount importance in the field of DNA damage.

Oxidation of adenine (**A**, see Figure 1a) has attracted the attention of the scientific community since the 1970s.[22−24] On the basis of the pioneer works carried out by Van Hemmen[24] and O'Neill and co-workers,[25] Vieira and Steenken proposed two main pathways for the **A** + •OH reaction in a series of papers reported in the late 1980s:[16−18] (a) addition to the C4 position followed by dehydration of the corresponding **A4OH** adduct to produce (A−H)• and (b) addition to the C8 position followed by opening of the imidazole ring. The first process was tracked by the decay in optical density (OD) at ∼400 nm, considering that this absorption signal is produced by the **A4OH** radical, while the ring opening of the **A8OH** species was assigned to the increase in OD at ∼330 nm (see Figure 1b). The assignments were based on the O_2 quenching rates of both ∼330 and ∼400 nm bands, assuming faster reactions of **A4OH** and **A8OH** toward O_2 as compared to the **A5OH** quenching.[16,18] This assumption was based on the distinct estimated spin-density distributions among carbon and heteroatoms for each radical. No real evidence supports, however, the hypothesis. Difficulties in the determination of the C4/C5 regioselectivity arise not only from the fast decomposition of the **A4OH**/**A5OH** species, which undergoes ⁻OH loss on the microsecond scale, hampering its experimental detection. The chemical structure of **A** also complicates the resolution, since the C4 and C5 positions do not allow substitutions, making the synthesis of photolabile precursors of C4- or C5-centered radicals impossible, a strategy recently used in pyrimidine NBs (see ref 26 and references cited therein).

Received: October 1, 2016
Published: December 13, 2016

DOI: 10.1021/acs.joc.6b02393
J. Org. Chem. 2017, 82, 276−288

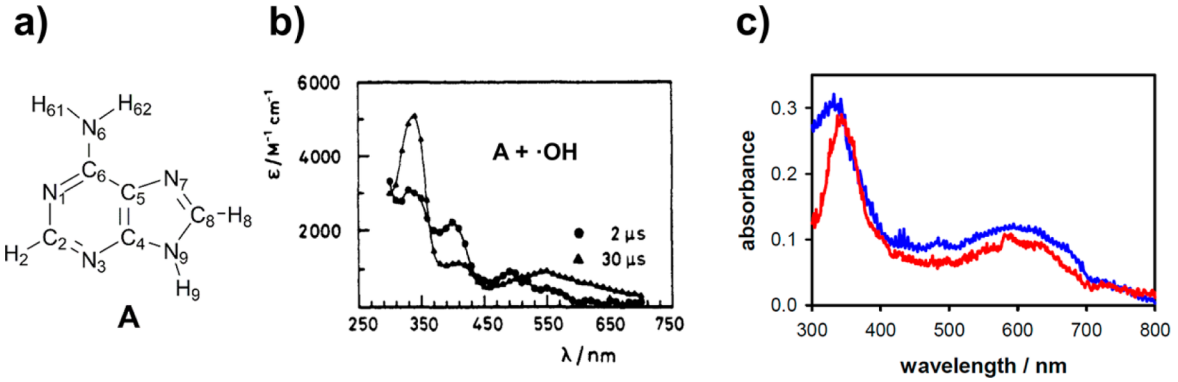

Figure 1. (a) Structure and atom numbering of adenine (**A**). (b) Experimental UV−vis spectra of **A** at 2 (circles) and 30 (triangles) μs after reaction with $^{\bullet}$OH. Reprinted with permission from ref 16. Copyright 1990 American Chemical Society. (c) Experimental UV−vis spectra of $\mathbf{A}^{\bullet+}$ (red line) and **ANH** (blue line). Reprinted with permission from ref 28. Copyright 2016 American Chemical Society.

Both **A4OH** and **A5OH** are transformed to the oxidant $(A-H)^{\bullet}$ species, identified as the radical dehydrogenated from the $-NH_2$ group (**ANH**). Kobayashi[27] and Banyasz et al.[28] reported the UV−vis spectrum of **ANH** (see blue circles in Figure 1c). It is characterized by a sharp signal at the ∼300−350 nm region and a broad band at the ∼450−550 nm. Other research groups reported similar spectra.[29−32] It becomes apparent from the comparison of the recorded spectra displayed in Figure 1b,c that the characterization of the ring-opening reaction carried out by Vieira and Steenken[16] is questionable since the authors tracked the **A8OH** breakage at ∼330 nm, where the abundant radical **ANH** exhibits an intense absorbance. In addition, the reported O_2 quenching rates, pH dependencies, activation parameters, substituent effects, and conductance experiments[18] indicate that the processes occurring at ∼330 and ∼400 nm are of a *different* nature.[16] This fact rules out the interpretation that decomposition of **A4OH**, previously ascribed at ∼400 nm, also causes the buildup at ∼330 nm (due to formation of **ANH**). An important question arises at this point: if the buildup at ∼330 nm is caused by **ANH**, as shown in Figure 1c, what is responsible for the decay at ∼400 nm? It seems therefore timely to reinterpret the experimental recordings in light of modern theoretical calculations.

In the last years, a series of quantum-chemistry studies have contributed in the understanding of the purine NBs reaction with OH radicals.[33−35] Density functional theory (DFT) calculations using the ωB97X-D functional (hereafter, DFT/ω-B97X-D method) carried out by Milhøj and Sauer[34] suggested that dehydrogenations from both the $-NH_2$ group and C2 positions are preferred over H atom loss from the C8 position. Analysis of the reaction rate constants including tunneling effects indicated that only addition to the C8 position competes with the dehydrogenations, and both addition and H atom abstractions have the same contributions to the overall **A** + $^{\bullet}$OH rate constant. Slower reaction constants were obtained when including solvent effects.[35] Naumov and von Sonntag[36] documented in 2008 the energetics of the dehydration process of the hydroxyl radical adducts of **A** and some ring-opening intermediates employing the DFT/B3LYP method. The H atom loss was found to be exothermic for the **A4OH** and **A5OH** adducts but clearly endothermic for the **A8OH** radical. Three intermediates for the ring-opening reaction of the **A8OH** were considered: **A8EN**, **A8FORM**, and **A8N9** (see Figure 2). Only **A8FORM** was reported to be energetically more stable than the **A8OH** adduct.

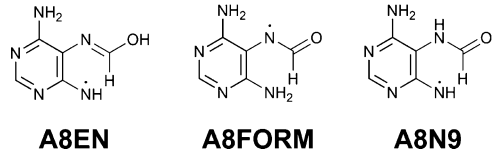

Figure 2. Imidazole-ring-opened radicals studied by Naumov and von Sonntag.[36]

Munk et al.[37] studied the ring-opening processes of the $^{\bullet}$OH adduct of guanine at the C8 position (G8OH) and reported a water-assisted proton transfer from the −OH moiety to the N7 atom to form the corresponding O-centered radical. A few years later, Sevilla and co-workers[38] studied in detail the dehydration mechanism of the G4OH and the G5OH adducts of guanine, ascribing the initial $^{-}$OH loss to the presence of a metastable complex with zwitterion character, followed by deprotonation of the aforementioned G4OH/G5OH adducts. The authors concluded that both dehydration and direct H atom abstraction channels are competitive.[38]

Theoretical calculations have been also used to interpret the UV−vis spectra of the radical intermediates. Cheng et al.[33] assigned the signals recorded experimentally at ∼330 and ∼400 nm[16] to the **ANH** species (i.e., the dehydrogenated adenine at N^6 position) on the basis of time-dependent (TD)-B3LYP calculations. However, the assignation cannot be correct since it is demonstrated in the experiments that the signals are caused by different species.[16,18] Finally, the authors suggested that the broad band at ∼520−650 nm could be caused by absorptions of the ring-opened radical intermediates.

To the best of our knowledge, high-level ab initio multireference computations on the excited states of the radical intermediates have not been carried out in the previous studies. Moreover, a satisfactory agreement between experimental interpretations and theoretical calculations on the **A** + $^{\bullet}$OH reaction mechanisms has not been yet reached. Disagreements arise from the regioselectivity of the first-step reaction. Early experimental works proposed that addition to C4 position is the preferred pathway,[16−18,25] whereas theoretical estimations favor the C5 position.[34,39] In the present paper, we report evidence that supports a more favorable and competitive addition to the C5 and C8 positions, and we clearly demonstrate that the C4 channel must be considered a

DOI: 10.1021/acs.joc.6b02393
J. Org. Chem. 2017, 82, 276−288

Scheme 1. Chemistry of the •OH Addition to A[a]

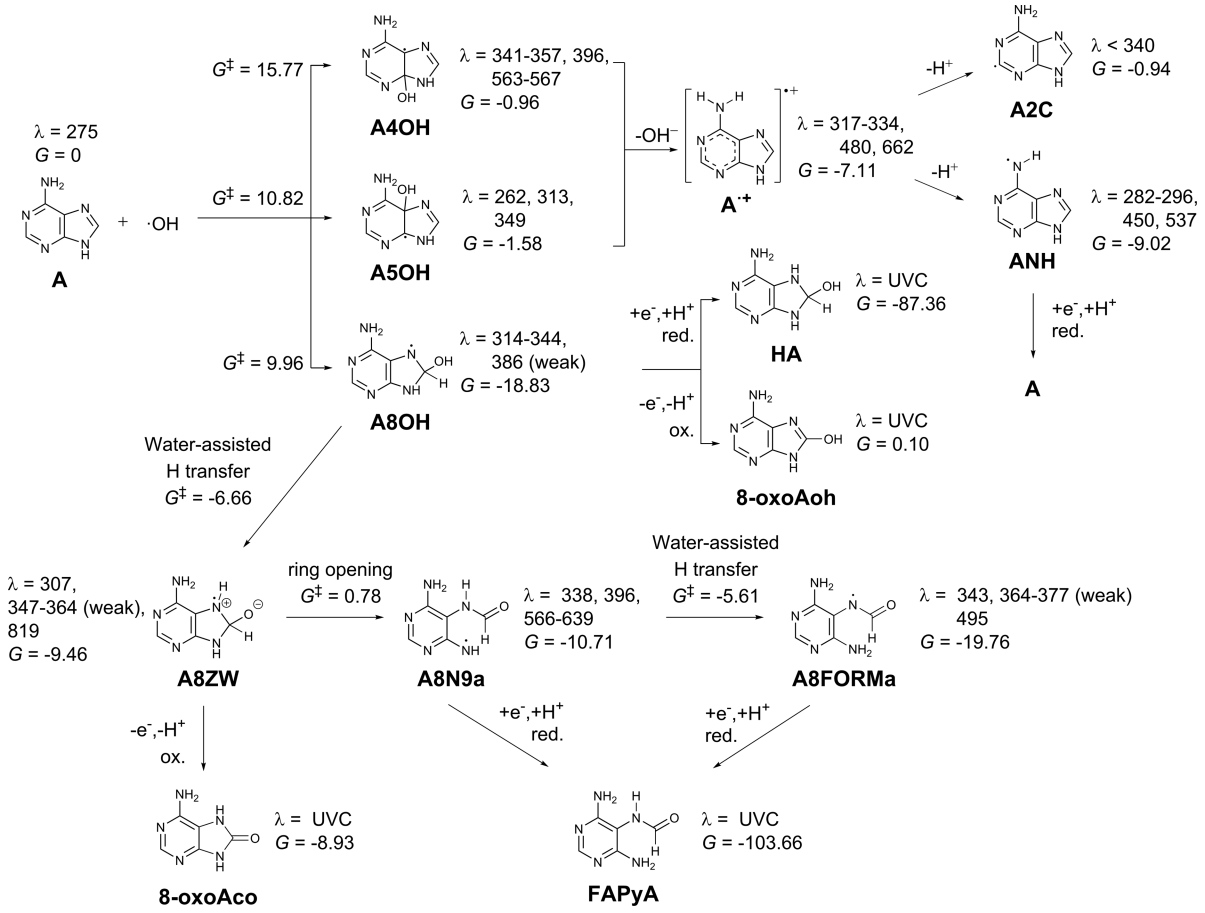

[a]*G* and *G*‡ energies (kcal/mol) are computed with the M06-2X-(PCM) method, except the *G* values of **A**•+, **ANH**, and **A2C**, which are computed using the CCSD(T)-(PCM)//M06-2X-(PCM) approach. All vertical absorptions (λ, in nm) are calculated with the CASPT2//CASSCF protocol. The reported energies of the radical intermediates are relative to the **A** + •OH reactants. **A8ZW** is complexed with three water molecules (see text). *G* energies of the oxidized systems **8-oxoAoh** and **8-oxoAco** are calculated according to the equation A + •OH → 8-**oxoAoh**/**8-oxoAco** + •H. *G* energies of the reduced systems **HA** and **FAPyA** are calculated according to the equation **A** + •OH + •H → **HA**/**FApyA**.

significantly minor pathway. Optical changes at ∼400 nm are explained in terms of the oxidation/reduction of the ring-opened **A8OH** derivatives, while the intense band recorded at ∼330 nm is mainly assigned to the absorbance of **ANH** species. The complete mechanism for the formation of the **8-oxoA**[40,41] and **FAPyA**[42] mutagens from the **A8OH** radical is also documented. Finally, by using data from product analysis studies[16] and theoretical kinetic constants, it is estimated that in water solution approximately the ∼44.5% of the total •OH yield adds to **A** (∼26.5% to C5 and ∼18% to C8), whereas the remaining ∼55.5% is expected to react through one-electron oxidation and H atom abstraction mechanisms.

METHODS AND COMPUTATIONAL DETAILS

The Minnesota M06-2X functional[43] as implemented in the Gaussian 09 (D.01 revision) software package[44] in conjunction with the standard 6-31++G(d,p) basis set has been used for the computations of the thermodynamic (*G* and *G*‡) parameters of the reactions.[45,46] Frequency calculations using the harmonic oscillator approximation have been conducted in order to identify the corresponding stationary points and to obtain the zero-point vibrational energies. The nature of the transition states (TSs) have been confirmed by the identification of a single imaginary frequency corresponding to the vibrational mode along the reaction coordinate. Additionally, the connectivity between the TSs and the corresponding reactants and products has been ensured by means of intrinsic reaction coordinate (IRC) calculations. Further optimizations have been performed on the IRC final structures in order to obtain fully relaxed geometries. The rigid-harmonic oscillator-ideal gas approximation, which has been demonstrated to provide acceptable values for thermodynamic properties,[47] has been used to compute the Gibbs energies at 298 K and 1 atm. The solvent effects have been taken into account both in the geometry optimizations and the final energies by means of the integral equation formalism-polarized continuum model (IEF-PCM) method [hereafter, M06-2X-(PCM) method], using the Gaussian 09 (D.01 revision) default settings. Three explicit water molecules have been needed for an accurate description of the **A8OH** → **A8ZW** → **A8N9** transformations, while only one has been required for the **A8N9** → **A8FORM** reaction.

Energy corrections on top of the M06-2X-(PCM)-converged structures have been performed using the highly accurate coupled-cluster method with single, double, and perturbative triple excitations [CCSD(T)] also using the PCM model [hereafter, CCSD(T)-(PCM)//M06-2X-(PCM) methodology]. The M06-2X-(PCM) energies have been systematically compared with the CCSD(T)-(PCM)//M06-2X-(PCM) results obtained for the •OH addition at the C4 and C5 positions of **A** and subsequent dehydration processes (see Table S1 and Table 3), showing small deviations not significantly larger than 2 kcal/mol for the neutral systems, thus validating the less computationally expensive M06-2X-(PCM) level for the description of the •OH reactivity toward **A** (see Scheme 1 below). The DFT/M06-2X methodology is also in qualitative agreement with respect to ab

DOI: 10.1021/acs.joc.6b02393
J. Org. Chem. 2017, 82, 276−288

initio multiconfigurational calculations, as shown in a previous study of the $^{\bullet}$OH addition to uracil.[48] Electron-transfer reactions have been described using the CCSD(T)-(PCM)//M06-2X-(PCM) approach, which is able to reproduce the available experimental data with reasonable agreement (see eq 1 below).

Determination of the thermodynamic parameters of H^+ and $^-$OH species in water solution, which are poorly reproduced by quantum-chemistry methods due to the acid−base equilibrium of water, have required the use of experimental measurements of their solvation energies. Thereby, for H^+ the Gibbs energy in solution $G_{sol}(H^+)$ = $G_{gas}(H^+)$ + $\Delta G_{sol}(H^+)$ = −6.28 + (−264.61) = −270.89 kcal/mol (−0.4317 au) taken from the literature[49,50] has been used for the calculations involving protonations/deprotonations. This strategy has been successfully used in previous theoretical studies (see refs 49−51 and references cited therein). Other values of $\Delta G_{sol}(H^+)$ with discrepancies of 1 or 2 kcal/mol have been reported in the literature;[52−54] however, such differences do not affect the conclusions of the present work. In the case of $^-$OH, the solvation energy obtained with the M06-2X-(PCM) method is $G_{sol}(^-OH)$ = −83.59 kcal/mol (−0.1332 au), which is grossly smaller than the reported experimental value of $G_{sol}(^-OH)$ = −119.29 kcal/mol (−0.1901 au).[55] Therefore, the latter value has been used in the present calculations. On the contrary, the neutral $^{\bullet}$OH species in solution is well described using theoretical methods with the continuum model. Autrey et al.[56] reported that $\Delta G_{sol}(^{\bullet}OH)$ = −3.9 ± 0.3 kcal/mol (0.0062 ± 0.0002 au) using photoacoustic calorimetry and ab initio calculations, whereas the M06-2X-(PCM) method gives a similar value of −3.44 kcal/mol (0.0055 au).

Vertical absorption energies (VAEs) of the radical intermediates in vacuo have been computed with the highly accurate complete-active-space second-order perturbation theory (CASPT2)//complete-active-space self-consistent field (CASSCF) approach (hereafter, CASPT2//CASSCF methodology),[57−61] which means that the geometries are optimized with the CASSCF method[62] and the energies are corrected with the CASPT2 method[63,64] on top of the optimized structures. The atomic natural orbital (ANO) L-type with the contraction scheme C, N, O [4s3p1d]/H [2s1p] (hereafter, ANO-L 431/21) has been used throughout.[65] The CASSCF wave functions for the geometry optimizations have been built including in the CAS active space only the relevant π and π^* molecular orbitals (MOs) of the systems. VAE calculations have been conducted with the whole valence space in the CAS (for a detailed description of the CAS used in the systems see Figures S1−S3 and Table S2) and demanding 10 roots in the State-Average (SA)-CASSCF procedure. Computations of the **A4OH**, **A5OH**, and **A8OH** VAEs have been performed excluding the lone pair localized in the −OH group from the active space because it does not participate in the description of the low-lying excited states even when the number of roots is increased to 12 or the active space is enlarged to 14 MOs. The dynamic electron correlation has been computed with the CASPT2 method freezing the core orbitals during the perturbation step. A level shift of 0.2 au has been used in order to minimize the presence of weakly interacting intruder states, and the ionization-potential electron-affinity parameter has been set to 0.0 au. The effect of the number of roots demanded in the SA-CASSCF procedure on the CASPT2 energies have been studied in the **A5OH**, **A8OH**, **A8N9a**, and **A8FORMa** systems, varying from 8 to 12 roots (Tables S3−S6, respectively). Analysis of the results shows a convergence of the excitation energies (see Supporting Information). Oscillator strengths (f) have been computed according to the formula $f = \frac{2}{3}E_{VA}TDM^2$ where the TDM stands for the CASSCF transition dipole moment between the initial φ_1 and final φ_2 electronic states, and TDM = $\langle\varphi_1|\vec{d}|\varphi_2\rangle$, where $\vec{d}$ is the dipole moment operator. The present CASPT2//CASSCF computational approach has been demonstrated to provide accurate results compared to experimental recordings,[26] and has been previously used by the authors of the present work to correctly assign experimental transient absorption spectroscopy signals of uracil, thymine, and cytosine radicals.[26,66]

All of the multiconfigurational calculations have been performed with the MOLCAS 8 software package.[67]

RESULTS AND DISCUSSION

The most relevant reactions involved in the addition of $^{\bullet}$OH to **A** and the fate of the formed adducts are displayed in Scheme 1. For the sake of clarity, in the first section only the C4 and C5 addition channels will be considered. Next, addition to C8 position and subsequent ring-opening reactions will be discussed. Later, the experimental O_2 quenching rates and the pH dependencies of the optical signals will be rationalized on the basis of the present computations. Next, the yield of the $^{\bullet}$OH addition to **A** will be estimated from theoretical kinetic constants and previous product analysis studies. Finally, some comments regarding of the $^{\bullet}$OH reaction with **A** in biological DNA/RNA systems will be provided.

Addition to C4 and C5 Positions. According to the experimental literature,[16−18] OH radical adds preferentially to the C4 position of **A** to yield the corresponding **A4OH** radical (∼65%), whereas addition to the C5 position has been considered a minor path (∼16%). The corresponding G and $G^{\ddagger}$ for these reactions are displayed in Scheme 1. The TS for the $^{\bullet}$OH addition to the C4 atom ($G^{\ddagger}$ = 15.77 kcal/mol) lies ∼5 kcal/mol above the one for the C5 atom ($G^{\ddagger}$ = 10.82 kcal/mol), indicating thus a marked preference for the C5 addition. These results show discrepancies with experimental interpretations,[16−18] while are in agreement with previous calculations using the ωB97X-D functional.[34,68] Moreover, the relative energies of **A4OH** and **A5OH** adducts are very similar to that of the **A** + $^{\bullet}$OH reactants, and therefore, thermodynamic parameters do not justify preference for one or the other.

The relevant CASPT2 vertical absorption wavelengths of **A4OH** and **A5OH** species are also displayed in Scheme 1, whereas the complete data are summarized in Tables S7 and S8 in the Supporting Information. Both radicals absorb at the ∼350 nm region; however, differences between **A4OH** and **A5OH** appear at the ∼400 nm zone. The $\mathbf{D_1} \rightarrow \mathbf{D_4}$ transition of the first compound, predicted at 396 nm, with f = 0.005 (see Table S7), could be responsible for the possible absorption at ∼400 nm. Therefore, **A4OH** seems to be a reasonable candidate to explain the decay observed at this wavelengths in the experiments (see Figure 1b).[16] However, this species has to be considered as a minor contributor to the signal, based on the fact that the TS energy computed for the C4 addition is significantly higher than the TSs for the other additions (see Scheme 1). To further support this conclusion, we have performed several theoretical studies on the TSs of the C4 and C5 addition channels, analyzing the stability of the results upon changing the methodology and upon modeling more accurately the solvation process actually occurring in water. The first analysis indicates that the result is independent from the theoretical method. Thus, accurate electronic structure calculations [see CCSD(T)-(PCM)//M06-2X-(PCM) results below, Table 3)] and previous computations with different functionals[34,39] corroborate the energy trend. Second, explicit solvation has been modeled at the DFT/M06-2X-(PCM) level including six molecules of water localized in the plane of **A**. Results indicate that the TS4 structure lies 4.97 kcal/mol *above* the TS5 one, being in full agreement with the M06-2X-(PCM) description without explicit solvent molecules. Analysis of the Mulliken charges of the converged structures indicate that the carbon atom that forms the C−OH bond have significant negative charges (−1.24 and −0.52 for the TS4 and the TS5 structures, respectively). The possible stabilization of this charge by an additional water molecule (having in total 7 water

DOI: 10.1021/acs.joc.6b02393
J. Org. Chem. 2017, 82, 276−288

molecules in the system), which could lead to a differential solvation of the TSs, has been appraised by computing the potential energy surface along the C−H_2O coordinate as displayed in Figures S4 and S5. Very small stabilizations (−1.13 vs −0.87 kcal/mol) have been computed for the systems, confirming the preference for the C5 channel. Moreover, dynamic effects not considered in this work are not expected to change this conclusion taking into account such small interaction energies between water and **A** found in this region.

A4OH and **A5OH** radicals lose a water molecule to give the corresponding **ANH** compound (see Scheme 1). On the basis of the absence of conductance changes on a microsecond scale, Vieira and Steenken[17] suggested that the two-step mechanism shown in Scheme 1 is ultrafast, proposing that the $^{-}$OH loss is coupled with the deprotonation of the radical cation $\mathbf{A}^{\bullet+}$. Later measurements of the deprotonation of adenine radical cation on a *nanosecond* scale[27] support Vieira and Steenken's observations. On the other hand, the $^{-}$OH loss was theoretically explained in guanine adducts by Sevilla and co-workers by the existence of a metastable complex.[38] *G* values for the $^{-}$OH loss from **A4OH** and **A5OH** and further deprotonation of $\mathbf{A}^{\bullet+}$ shown in Scheme 1 indicate an exergonic dehydration of the compounds. For the one-electron transfer reaction (eq 1)

$$A + {}^{\bullet}OH \rightarrow A^{\bullet+} + {}^{-}OH \qquad \Delta G = -7.11 \text{ kcal/mol} \qquad (1)$$

ΔG lies within the experimental range of $-10.8 \leq \Delta G \leq -6.00$ kcal/mol, obtained by subtracting the experimental one-electron oxidation potential of adenosine (32.8[69] − 37.6[70] kcal/mol) and that of $^{\bullet}$OH (43.6 kcal/mol).[71] Deprotonation of $\mathbf{A}^{\bullet+}$ to give **ANH** (eq 2) is also computed to be exergonic in −1.91 kcal/mol, which is comparable to the reported values of ≤1.4[72] (experimental) and −0.7[73] kcal/mol (theoretical):

$$A^{\bullet+} \rightleftarrows ANH + H^{+} \qquad \Delta G = -1.91 \text{ kcal/mol} \qquad (2)$$

The $\mathbf{A}^{\bullet+}$ species has two intense electronic transitions at the ∼330 nm region (see Scheme 1), $\mathbf{D}_1 \rightarrow \mathbf{D}_7$ and $\mathbf{D}_1 \rightarrow \mathbf{D}_8$, calculated at 334 and 317 nm (see Table S9), respectively. The associated *f* are 0.091 and 0.168, which are values significantly larger than those of the other radicals studied in this work. CASSCF dipole moment modules indicate that the $\mathbf{D}_1 \rightarrow \mathbf{D}_7$ transition should be slightly blue-shifted in water. On the other hand, the $\mathbf{D}_1 \rightarrow \mathbf{D}_5$ transition lies at lower energies (480 nm) and also has a large $f = 0.073$. On the basis of the dipole moment modules of the $\mathbf{D}_5$ (4.72 D) and the $\mathbf{D}_1$ (2.48) states, certain red shift due to solvent effects is predicted for this absorption. $\mathbf{A}^{\bullet+}$ also has some absorbance in the red region (662 nm), but the *f* of the corresponding transition is relatively small (see Table S9). The CASPT2 results for the optical properties of $\mathbf{A}^{\bullet+}$ are in agreement with recent experimental recordings[27,28] (see red lines of Figure 1c) and theoretical calculations. Banyasz et al.[28] have reported the excitation energies of $\mathbf{A}^{\bullet+}$ computed with TD-M05-2X-(PCM)/6-31+G-(d,p) method including five explicit water molecules. Four electronic transitions were estimated within the 300−700 nm range, in particular at 303, 327, 331, and 620 nm, after red-shifting the computed values by 0.55 eV to match the experimental spectrum. Both CASPT2 and TDDFT methods are coincident in the description of the optical absorptions at ∼330 and ∼600 nm region, however, the multiconfigurational approach provide an additional bright transition at 480 nm. Experimental recordings[27,28] show a small shoulder at the ∼500 nm zone, supporting therefore the CASPT2 results. Conversely, TD-DFT computations better reproduce the tail of the spectrum at long wavelengths (>800 nm).[28]

ANH (see Scheme 1) displays several relevant electronic transitions in the UV−vis region, namely $\mathbf{D}_1 \rightarrow \mathbf{D}_4$, $\mathbf{D}_1 \rightarrow \mathbf{D}_5$, $\mathbf{D}_1 \rightarrow \mathbf{D}_7$, $\mathbf{D}_1 \rightarrow \mathbf{D}_8$, and $\mathbf{D}_1 \rightarrow \mathbf{D}_9$, predicted at 537, 450, 296, 288, and 282 nm, with associated *f* of 0.015, 0.019, 0.005, 0.098, and 0.041, respectively (see Scheme 1 and Table S10). For all of the absorptions, the CASSCF dipolar moment modules of the excited state are significantly larger than that of the $\mathbf{D}_1$ ground state, indicating red shifts of the vertical absorptions toward the experimental values. The strongest shifts are expected for the high-energy absorptions since the difference in the dipolar moment module between the excited and the ground state is up to ∼3 D. The optical properties of **ANH** agree well with previous experimental recordings, which show broad absorption bands at ∼300−350 and ∼500−700 nm.[27−29] The TD-M05-2X-(PCM)/6-31+G(d,p) results documented by Banyasz et al.[28] are in reasonable agreement with the present multiconfigurational outcomes. The authors reported two electronic transitions between 400 and 800 nm, one at 527 nm and other at ∼670 nm. The former absorption agrees well with the bright CASPT2 transition at 537 nm, whereas in the latter region the multiconfigurational approach yield two bands (at 740 and 640 nm) significantly darker. In contrast, the small shoulder peaking at ∼450−500 nm observed in the experiments[27,28] is better explained with the CASPT2//CASSCF methodology, which predicts an electronic transition at 450 nm.

It becomes apparent from the present theoretical results and previous experimental recordings[27,29] that the buildups observed at ∼330 and ∼520−650 nm are caused by the absorptions of **ANH** species. Absorption of $\mathbf{A}^{\bullet+}$ at pH ∼7 is discarded since equilibrium (eq 2) is almost completely favored in the **ANH** + H^+ direction, as demonstrated by nanosecond spectroscopy experiments.[27]

Assignation of the signals at ∼330 and ∼520−650 nm to **ANH** excitations questions the experimental interpretations of Vieira and Steenken.[16−18] The authors followed the ring-opening reactions by means of the optical changes at ∼330 nm; however, they were tracking the formation of **ANH** instead. Three mechanisms compete in the formation of this radical, which accounts for ∼81% of the $^{\bullet}$OH total yield:[16] (a) dehydration of **A5OH** (Scheme 1), (b) one-electron oxidation of **A** followed by deprotonation of $\mathbf{A}^{\bullet+}$ (eqs 1 and 2, and (c) direct hydrogen abstraction from the $-NH_2$ group (not studied in the present work). Even though a precise determination of the dominant mechanism is challenging, recent advances highlight the hydrogen abstraction role in the $^{\bullet}$OH reaction with purines[28,33,68,74] suggesting that it could represent a half of the total $^{\bullet}$OH reaction with A.[68]

Dehydrogenation from the C2 position gives rise to **A2C**, which lies ∼3−4 kcal/mol above the **ANH** compound and is transparent in the UV−vis region (see Scheme 1 and Table S11).

Addition to C8 Position and Ring-Opening Reactions. OH radical adds to the C8 position of **A** forming **A8OH** (see Scheme 1) with an experimental yield of ∼18% determined by product analysis.[16] The Gibbs activation barrier for this reaction is 9.96 kcal/mol, significantly lower than that of the addition to C4 position and quasi isoenergetic with the barrier height of the C5 channel (Scheme 1). In contrast to the **A4OH** and **A5OH** isomers, **A8OH** is significantly more stable than the **A** + $^{\bullet}$OH reactants ($G = -18.83$ kcal/mol, see Scheme 1), and it

DOI: 10.1021/acs.joc.6b02393
J. Org. Chem. 2017, 82, 276−288

represents a key structure in the oxidation of **A**. Whereas addition to C4 and C5 could be considered as reversible reactions, oxygenation of C8 position must be contemplated as irreversible, serving as a chemical marker of DNA oxidation.[13] Two products are of special relevance for this purpose, namely **8-oxoA** and formamidopyrimidine-A (**FAPyA**) lesions.[42,75] The mutagenic capability of both compounds has been extensively demonstrated in the literature.[40,76]

By comparison of the Gibbs energies of $\mathbf{A}^{\bullet+}$ and **A8OH** displayed in Scheme 1, dehydration of the latter compound is predicted to be highly endergonic (ΔG = 15.01 kcal/mol), in agreement with Vieira and Steenken early interpretations[16,18] and Naumov and von Sonntag conclusions.[36] Instead, **A8OH** undergoes a series of relatively intricate ring opening reactions, where the intermediates are eventually oxidized to yield **8-oxoA** (**oxoAoh**, enol form, or **8-oxoAco**, keto form) or reduced to produce **FAPyA**. It is not surprising then that **8-oxoA** is formed in higher yields than **FAPyA**[15] since the reaction medium is oxidizing due to the presence of **ANH**,[16] which has oxidant character according to eq 3:

$$\mathrm{ANH} + e^- + H^+ \rightarrow \mathrm{A} \qquad (3)$$

A8OH radical has a bright $\mathbf{D}_6$ state lying at 344 nm (see Scheme 1 and Table S12). Thus, it absorbs in the same UVA region as that of **A5OH**. It is therefore reasonable to ascribe the band at ∼330 nm recorded 2 μs after the generation of $^{\bullet}$OH[16,18] to the optical absorptions of **A8OH**, **A5OH**, and **ANH** species.

A number of pathways leading from the **A8OH** radical to the final products **HA**, **8-oxoAoh**, **8-oxoAco**, and **FAPyA** have been studied in the present work. Oxidation of **A8OH** to give **8-oxoAoh** (see Scheme 1) was employed by Vieira and Steenken[16] to quantify the oxidation at C8 position using the strong oxidant $[Fe(CN)_6]^{-3}$ and HPLC for the product analysis, assuming that oxidation by $[Fe(CN)_6]^{-3}$ occurs before ring-opening processes. In the present study, we have estimated the redox properties of **A8OH** by computing the Gibbs energy differences involved in the process of removing or adding an electron (e^-) and a proton (H^+). Nevertheless, the actual redox reaction involving the radical will also depend on the redox potentials of the species present in the environment. Reduction of **A8OH** yields the 7-hydro-8-hydroxypurine **HA**, as displayed in Scheme 1. The thermodynamics of the reaction are highly exergonic, albeit **HA** is not observed in the experiments probably due to further tautomerization to the more stable **FAPyA** isomer.[37,42] Three tautomerization mechanisms have been computed in the present work (see Scheme S1): (i) unimolecular ring-opening followed by H transfer from the oxygen to the N9 atom (see Figure S6 for the IRC computations), (ii) protonation at the N9 position followed by deprotonation from the oxygen atom, and (iii) deprotonation from the oxygen atom followed by protonation at the N9 position. Process i can be considered slow due to the high activation barrier ($\Delta G^{\ddagger}$ ∼ 35 kcal/mol), whereas process ii is predicted to be more favorable based on the computed energy of the protonated intermediate (ΔG = 17.72 kcal/mol). According to these results, it is expected that acid conditions will accelerate the **HA** → **FAPyA** tautomerization. The possible explicit participation of water molecules has also been explored; however, neither the reaction complex nor the TS have been encountered, probably due to the low hydrogen acceptor capacity of the N9−H position. The closed-shell compound **HA** absorbs at the UVC region of the electromagnetic spectrum and consequently lies out of the **A** + $^{\bullet}$OH spectrum displayed in Figure 1b.

Ring opening of **A8OH** involves the rupture of either the C8−N7 or the C8−N9 bonds. The former breakage is the precursor of the 2,5-**FAPyA** compound (see ref 37 for guanine analogues), whereas the second scission leads to the **FAPyA** lesion isolated from oxidized DNA.[42,77] For this reason, in the present work we will focus only on the C8−N9 bond break. Structures, energetics of the most favorable intermediates and products, as well as the vertical absorptions are displayed in Scheme 1. The water-assisted proton transfer from the −OH group to the N7-centered radical proposed by Munk et al.[37] in G8OH radical has been studied for **A8OH**. The number of explicit water molecules included in the calculations has a significant impact on the activation Gibbs energy of the reaction, as previously noted by Munk et al.[37] Thereby, the inclusion of a single water molecule which explicitly catalyzes the double proton transfer lead to a $\Delta G^{\ddagger}$ = 16.87 kcal/mol. However, addition of three explicit water molecules, two of them participating in the triple proton transfer and other one stabilizing the exocyclic $-NH_2$ group decreases the activation barrier to $\Delta G^{\ddagger}$ = 12.17 kcal/mol (see Scheme 2). In this

Scheme 2. Water-Assisted Triple Proton Transfer from A8OH to A8ZW[a]

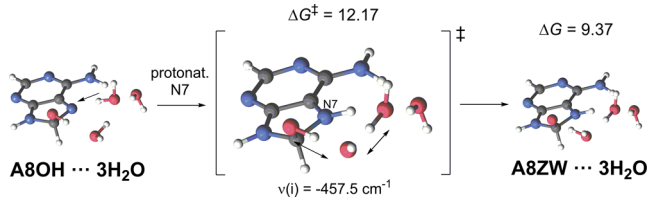

[a] ΔG and $\Delta G^{\ddagger}$ parameters (kcal/mol) are computed with the M06-2X-(PCM) method. Thermodynamic values of the **A8ZW**···$3H_2O$ complex are relative to the **A8OH**···$3H_2O$ structure (left).

mechanism (see IRC profile in Figure S7), protonation at the N7 position takes place as the system approaches to the saddle point, which consist of a double proton transfer between water molecules. As a result, the **A8ZW**···$3H_2O$ complex is formed, with G = −9.46 kcal/mol (see Scheme 1). Among the compounds studied in this work, **A8ZW** is the only one which has electronic transitions below 1 eV; however, the probability is low (see Table S13). Two relevant $\mathbf{D}_1 \rightarrow \mathbf{D}_4$ and $\mathbf{D}_1 \rightarrow \mathbf{D}_9$ transitions at 819 and 307 nm, with associated f values of 0.021 and 0.095, respectively, are predicted for **A8ZW** (see Scheme 1). Thus, this radical might contribute to the ∼330 nm band recorded experimentally at 30 μs (see Figure 1b).[16] On the other hand, other reaction pathways like the direct β-fragmentation of the C8−N9 bond of **A8OH** (see Scheme S2) or the 1,2 H-shifts in **A8OH** or **A8ZW** (see Scheme S3) are significantly more energetic.

Structures and Gibbs free energy changes related to the ring opening reaction of **A8ZW** are shown in Scheme 3, while energetics relative to the starting **A** + $^{\bullet}$OH reactants are displayed in Scheme 1. Thus, C8−N7 bond cleavage leads to the more stable intermediate **A8N9a** with a $\Delta G^{\ddagger}$ = 10.24 kcal/mol. The thermally accessible barrier at room temperature for the ring-opening reaction and the more stable **A8N9a** species makes this pathway favorable. In the presence of an adequate e^- and H^+ donor, **A8N9a** can be reduced to the more stable closed-shell system **FAPyA**. On the other hand, **A8ZW** can be

DOI: 10.1021/acs.joc.6b02393
J. Org. Chem. 2017, 82, 276−288

Scheme 3. Ring-Opening Reaction of A8ZW[a]

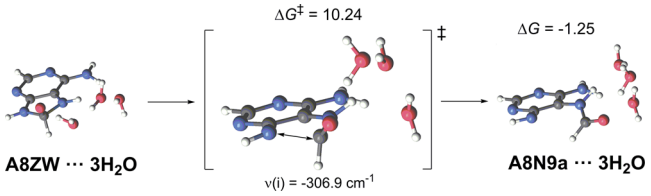

[a]ΔG and $\Delta G^{\ddagger}$ parameters (kcal/mol) are computed with the M06-2X-(PCM) method. Thermodynamic values of the **A8N9a**···$3H_2O$ complex are relative to the **A8ZW**···$3H_2O$ structure (left).

oxidized to **8-oxoAco** with a Gibbs free energy of −8.93 kcal/mol with respect to the starting **A** + $^{\bullet}$OH reactants (see Scheme 1). This compound is significantly more stable than its tautomer **8-oxoAoh**. The fate of **A8OH** is therefore governed by the presence of oxidants (yielding **8-oxoA**) or reductants (yielding **FAPyA**) in the reaction medium. The relatively large amount of **ANH**, an oxidizing agent (see eq 3), points to a more probable formation of **8-oxoA**, which agrees with the 5:2 ratio of **8-oxoA**/**FAPyA** determined experimentally.[16]

Spectroscopy of **A8N9a** is very interesting because it absorbs in the three regions of interest (~330, ~400 and ~520−650 nm);[16] see Scheme 1. The relevant transitions are $\mathbf{D_1} \rightarrow \mathbf{D_2}$, $\mathbf{D_1} \rightarrow \mathbf{D_6}$, and $\mathbf{D_1} \rightarrow \mathbf{D_8}$, predicted at 639, 398, and 338 nm, with associated *f* values of 0.012, 0.013, and 0.048, respectively (see Table S14). Analysis of the dipole moment module of the excited and ground states reveals that the two latter absorptions will be red-shifted in water solution. Therefore, in light of these CASPT2 results, the $\mathbf{D_1} \rightarrow \mathbf{D_6}$ transition of **A8N9a** can be safely assigned to the band observed at ~400 nm.

The detailed reaction mechanism of **A8N9a** to produce the more stable **A8FORMa** species is displayed in Scheme 4. The

Scheme 4. Water-Assisted Tautomerization from A8N9b to A8FORMb[a]

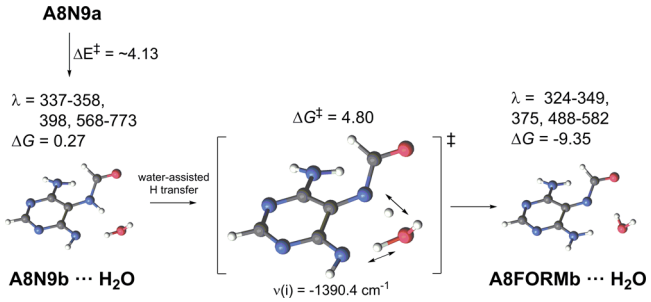

[a]G and $G^{\ddagger}$ parameters (kcal/mol) are computed with the M06-2X(PCM) method, whereas vertical absorptions (λ, in nm) are calculated with the CASPT2//CASSCF protocol in the absence of any water molecule.

A8N9b rotamer is involved in the process, with a rotation barrier estimated to be ~4 kcal/mol (see Figure S8). **A8N9b** can be transformed to **A8FORMb** through a low-energy water-assisted H transfer process ($\Delta G^{\ddagger}$ = 4.80 kcal/mol). The process is significantly exergonic, and the reverse activation barrier is of 14.15 kcal/mol. **A8FORMa** has two intense $\mathbf{D_1} \rightarrow \mathbf{D_7}$ and $\mathbf{D_1} \rightarrow \mathbf{D_8}$ transitions at 333 and 310 nm, with associated *f* values of 0.091 and 0.054, respectively (see Table S16). These transitions contribute to the band recorded at the ~330 nm region (see Figure 1b).[16] In addition, the $\mathbf{D_1} \rightarrow \mathbf{D_5}$ absorption computed at 377 nm and slightly red-shifted in water is expected to contribute to the experimental shoulder centered at ~400 nm.[16] No significant differences between the spectroscopic features of the **A8N9** and **A8FORM** rotamers are noted (see Tables S14−S17).

From the reaction mechanisms shown in Schemes 1−4, it is reasonable to conclude that **A8OH** undergoes relatively fast (microsecond scale) ring-opening reactions according to the **A8OH** → **A8ZW** → **A8N9** → **A8FORM** transformations (see Figure 3). The TS from **A8ZW** to **A8N9a** is the highest energy

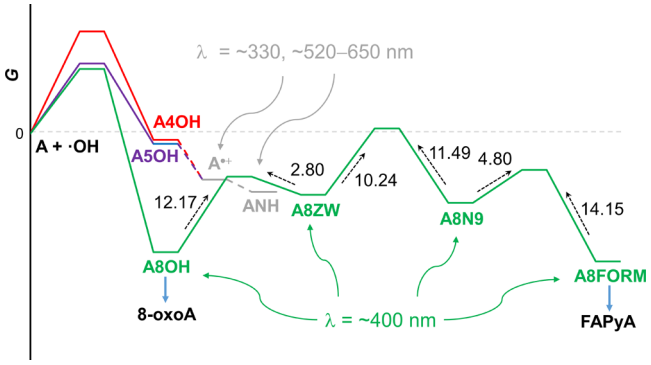

Figure 3. Energetics (in kcal/mol) of **A4OH**/**A5OH** dehydration and **A8OH** ring-opening processes. Dashed lines are used to connect the Gibbs energies of two species.

structure in this process ($G^{\ddagger}$ = 0.78 kcal/mol) and must overcome two consecutive barriers of 12.17 (**A8OH** → **A8ZW**) and 10.24 (**A8ZW** → **A8N9**) kcal/mol. Despite the fact that **A8ZW** represents a stabilization of 3.00 kcal/mol from the first TS, the overall **A8OH** → **A8N9** transformation can be considered the bottleneck of the process that produces the most stable **A8FORM** radical. Nevertheless, it is expected that this energy barrier can be surmounted at neutral pH and room temperature, which agrees with the fact that **FAPyA** is measured after $^{\bullet}$OH reaction with **A** (~2%).[16] Tunneling effects can be important in the acceleration of the **A8OH** → **A8ZW** transformation and other hydrogen or proton transfer. Meanwhile, acid conditions are also expected to facilitate the process (see below). On the other hand, the **A8FORM** ring closure to yield **A8OH**, although possible, should be considered slower on the basis of the 14.15 kcal/mol energy barrier computed for its transformation to **A8N9** (see Scheme 4 and Figure 3). Even though the intermediates **A8ZW** and **A8N9** are going to be oxidized or reduced to some extent, energetics favor **A8OH** and **A8FORM** structures. The finding is in agreement with previous suggestions[36,72] and confirms these radicals as the main precursors of **8-oxoA** and **FAPyA** mutagens, respectively. Moreover, according to the optical properties computed for the radicals oxygenated at the C8 position (see Scheme 1), transformation of these intermediates to the closed-shell systems **8-oxoA** and **FAPyA** is predicted here to cause the *decay* in OD recorded at ~400 nm from 2 to 30 μs (see Figure 1b).[16] All the oxidized or reduced final products studied in this work absorb at UVC or shorter wavelengths (see Tables S20−S23).

On the Quenching of A4OH, A5OH, and A8OH by O_2. O_2 is often used to trap organic radicals, and it is especially useful to study mixtures of species with different oxidation rates. The **A4OH**/**A5OH**/**A8OH** formation ratio from **A** and the OH radical[16] was inferred from experimental data based on

DOI: 10.1021/acs.joc.6b02393
J. Org. Chem. 2017, 82, 276−288

their different reactivity toward O_2. Vieira and Steenken assumed that **A5OH** is more reactive toward oxygen as compared to **A4OH** and **A8OH** because a larger spin density distribution among carbon atoms should appear in the first radical, whereas in the second and the third ones more spin density should lie on the nitrogen atoms.[18] The present calculations of the spin-density distributions using the Mulliken approach (Table S24) agree only partially with the assumptions of Vieira and Steenken.[18] Whereas **A5OH** shows significant spin density over the C2, C4, and C6 positions (and small on N^6 atom), **A4OH** does not have unpaired electron density among the N1 and N3 positions, and thus, it should behave as a carbon-centered radical. On the other hand, **A8OH** has a spin density of 0.48 at N7 position and makes this species a more clear N-centered radical. Despite the small discrepancies between Vieira and Steenken assumptions for the spin densities[18] and the present Mulliken values, the energy barriers of the **A4OH**, **A5OH**, and **A8OH** reactions with O_2 computed in this work (see Table S24 and Figures S9−S17) agree well with the reactivity trend suggested in the experimental studies.[18] The oxidation barriers are 2.76−3.92 kcal/mol for **A5OH**, 6.21−7.56 kcal/mol for **A4OH**, and 10.61−15.97 kcal/mol for **A8OH**. Additionally, **A8N9** has similar energy barrier heights as compared to those of **A8OH** (Figures S18 and S19, 11.10−13.63 kcal/mol), whereas **ANH** and $\mathbf{A}^{\bullet+}$ have activation energies (see Figures S20−S27).

In the original experimental report,[16] the authors were not able to explain the quenching rate constants (k_{O2}) of the optical signals at ∼330 and ∼400 nm due to incorrect spectroscopic ascriptions of the optical bands.[16] However, the study using the CASPT2//CASSCF method and the reaction mechanisms proposed in this work allow to rationalize the experimental data. The k_{O2} values determined by Vieira and Steenken[16] are summarized in Table 1. The signal at ∼400 nm, assigned here to the **A8OH/A8N9/A8FORM** radicals, has a k_{O2} of 1.0×10^9 M^{-1} s^{-1}, which is slower than the rate related to the ∼330 nm band ($k_{O2} = 4.0 \times 10^9$ M^{-1} s^{-1}). The latter band is ascribed to the dehydration of **A5OH** to form **ANH**, which is the process responsible for the buildup at ∼330 nm. Taking into account that the **A5OH** + O_2 reactions have the lowest energy barriers (∼2.76 to ∼3.92 kcal/mol), it is reasonable to conclude that the "fast" quenching of the ∼330 nm signal is caused by the **A5OH** reaction with O_2 *preventing* its transformation to **ANH**, giving rise to a number of peroxide derivatives. **A8OH** and **A8N9** radicals will undergo similar reactions, however, their reaction with O_2 is slower (as demonstrated by the theoretical calculations), which explains the "slow" quenching measurement recorded at ∼400 nm (see Table 1). Hence, a coherent interpretation of both theoretical and experimental findings[16] has been reached in this work.

Table 1. Interpretation of the Absorption Band Quenching at ∼330 and ∼400 nm and Measured k_{O2} at Both Wavelengths

λ (nm)	k_{O2}[a] (M^{-1} s^{-1})	early interpretation[a]	present interpretation
∼400	1.0×10^9	A4OH + O_2	A8OH/A8N9/A8FORM + O_2
∼330	$4.0 \pm 1 \times 10^9$	A8OH + O_2	A5OH + O_2

[a]Reference 16.

On the pH Dependence of the ∼400 and ∼330 nm Signals. The impact of pH on the optical signals of the **A** + $^{\bullet}$OH reaction provides valuable information in the elucidation of the reaction mechanisms and allows the identification of species relevant at pH values close to biological conditions. pH dependences of the buildup at ∼330 nm (assigned to the production of $\mathbf{A}^{\bullet+}$/**ANH** by dehydration of **A5OH**) and the decay at ∼400 nm (disappearance of **A8OH/A8N9/A8FORM** by oxidation/reduction reactions) were reported by Vieira and Steenken[16] and are reproduced in Figure 4a. The buildup rates at ∼330 nm increase at low (<5) and at high (>10) pH. We suggest that dehydration of **A5OH** is accelerated at low pH due to protonation of the −OH group to form $-OH_2^+$, a much better leaving group, according to eq 4:

$$\mathbf{A5OH} + H^+ \rightarrow \mathbf{A5}{-}OH_2^+ \rightarrow \mathbf{A}^{\bullet+} + H_2O \qquad (4)$$

On the other hand, the buildup rate increase (∼330 nm) at basic pH can be explained in terms of deprotonation of two species: **A5OH** radical and $^{\bullet}$OH. First, we suggest that **A5OH** deprotonation occurs from the $-NH_2$ group (and possibly from other positions) *before* the $^{-}$OH loss, yielding the $\mathbf{A5N}^{-}$ anion derivative (see Scheme 5). The $-NH^{-}$ substituent is a stronger electron-donating group as compared to $-NH_2$ and consequently increases the electron density over the ring, facilitating the leaving of the $^{-}$OH anion to yield **ANH** species. This process differs from the dehydration mechanism shown in Scheme 1, where the deprotonation takes place *after* the $^{-}$OH loss.

It is also possible that another reaction mechanism derived from the deprotonation of $^{\bullet}$OH to produce $O^{\bullet-}$ could be

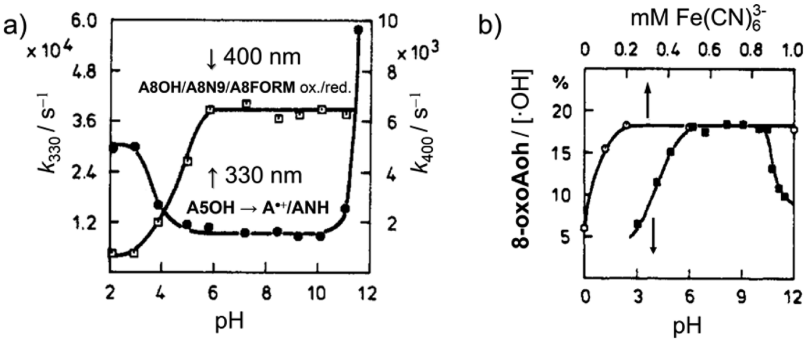

Figure 4. (a) pH dependence at 0 °C of the buildup rates at 330 nm (k_{330}) and the decay rates at 400 nm (k_{400}) for the adenosine + $^{\bullet}$OH reaction. [adenosine] = 0.4 mM. (b) Dependence of the **8-oxoAoh** yield (as percentage of $^{\bullet}$OH) on the concentration of $Fe(CN)_6^{3-}$ (circles) and on the pH in the presence of 0.8 mM $Fe(CN)_6^{3-}$ (squares). Adapted with permission from ref 16. Copyright 1990 American Chemical Society.

DOI: 10.1021/acs.joc.6b02393
J. Org. Chem. 2017, 82, 276−288

Scheme 5. Proposed Dehydration Mechanism of A5OH at Basic pH

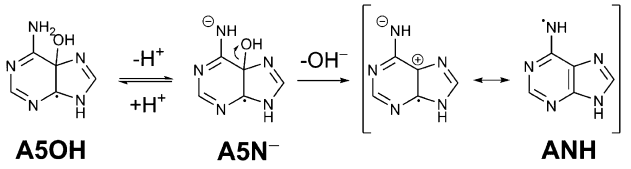

operative at large pH values (~11−12)[15] since the pK_a value of $^{\bullet}$OH has been reported to be 11.54.[78] This mechanism involves the H atom abstraction exerted by $O^{\bullet-}$ from the $-NH_2$ group of **A**, assuming that a fraction of unaltered **A** is present in the reaction medium. Scholes et al.[79] studied the reaction of $O^{\bullet-}$ with a series of nucleosides, concluding that the addition power of the radical anion decreases significantly but its H atom abstraction ability is barely affected. Consequently, it is reasonable to postulate that H atom abstraction from the $-NH_2$ substituent of **A**, yielding **ANH** and $^{-}$OH (eq 5), can take place at high pH values, increasing the OD buildup rate at ~330 nm:

$$A + O^{\bullet-} \rightarrow ANH + {}^{-}OH \quad (5)$$

The pK_a value of $^{\bullet}$OH (11.54) is in agreement with the drastic increase of the buildup apparent rate at ~330 nm recorded at pH ~11 (see Figure 4a) and the decrease of the **8-oxoAoh** yield observed at high pH (see Figure 4b), probably due to the weaker addition power of $O^{\bullet-}$ as compared to $^{\bullet}$OH.[79]

Vieira and Steenken[16] proposed a possible acid inhibition for the dehydration process through protonation at N1 or N^6 positions, which converts the electron-donating group $-NH_2$ into the electron-withdrawing substituent $-NH_3^+$. The authors argued that the reduction of electronic density over the ring moiety hampers the leaving of the $^{-}$OH anionic group. On the other hand, they also proposed a basic inhibition resulting from deprotonation from the alcohol group of **A5OH** to produce **A5O•**, blocking the $^{-}$OH elimination. We suggest that, although possible, these mechanisms have less impact on the dehydration rates of **A5OH** than those shown in eqs 4 and 5 and Scheme 5, in light of the experimental evidence displayed in Figure 4.

Regarding the rate decrease at low pH of the optical changes at ~400 nm (ascribed to oxidation/reduction of **A8OH**/**A8N9**/**A8FORM**), it can be related to the acid catalysis of the ring-opening reactions, which make the opened-ring radicals more accessible. It shall be demonstrated that disappearance of these opened-ring radicals (**A8N9** and **A8FORM**) is slower than that of the closed-ring tautomer (**A8OH**). We will only focus on the oxidizing processes since they are the main mechanisms of disappearance of the radicals, as concluded from previous product analysis studies.[16] First, the kinetics of the one electron reactions of the radical intermediates is studied. Second, the effect of acid pH on the reaction mechanisms is analyzed. Finally, a discussion about the oxidation mechanisms of the closed- vs opened-ring radicals is provided.

Table 2 summarizes the Gibbs activation barriers ($\Delta G_{ET}^{\ddagger}$) estimated using the Marcus theory[80] and the energies computed at the CCSD(T)-(PCM)//M06-2X-(PCM) level, according to eq 6

$$\Delta G_{ET}^{\ddagger} = \frac{\lambda}{4}\left(1 + \frac{\Delta G_{ET}}{\lambda}\right)^2 \quad (6)$$

Table 2. Gibbs Energies and Activation Barriers (kcal/mol) of Some Relevant One-Electron Transfer Reactions Operative at Neutral and Acid pH Values, Computed with the CCSD(T)-(PCM)//M06-2X-(PCM) Methodology

reaction	ΔG_{ET}	$\Delta G_{ET}^{\ddagger}$
Neutral pH		
ANH + **A8OH** → **ANH**$^{-}$ + **A8OH**$^{+}$	4.12	5.93
ANH + **A8N9** → **ANH**$^{-}$ + **A8N9**$^{+}$	20.93	21.74
ANH + **A8FORM** → **ANH**$^{-}$ + **A8FORM**$^{+}$	8.82	9.39
Acid pH		
A$^{\bullet+}$ + **A8OHH**$^{+}$ → **A** + **A8OHH**$^{2+}$	−15.10	0.67
A$^{\bullet+}$ + **A8N9H**$^{+}$ → **A** + **A8N9H**$^{2+}$	7.90	10.87
A$^{\bullet+}$ + **A8FORMH**$^{+}$ → **A** + **A8FORMH**$^{2+}$	−8.1	0.77

where λ is the relaxation energy of the final state (see Table S25 for the specific values) and ΔG_{ET} stands for the relative Gibbs energy between reactants and products. Results in Table 2 are qualitative, however, they help in the understanding of the mechanistic aspects of the $^{\bullet}$OH addition to **A**. At neutral pH (top rows), **ANH** is postulated as the main oxidant species as proposed by Vieira and Steenken,[16] whereas at acid pH (bottom rows) **ANH** is protonated to **A**$^{\bullet+}$ (pK_a = 4.2)[27] and the radical intermediates are protonated at the N1 or N9 positions (see Table S25 for structural details). It can be readily seen that **A8OH** radical is *more easily* oxidized than its opened ring tautomers **A8N9** and **A8FORM**. The oxidized radicals **A8OH**$^{+}$, **A8N9**$^{+}$, and **A8FORM**$^{+}$ exhibit electronic transitions at the ~370−430 nm region (see Tables S26−S28), and therefore, the spectroscopic decay tracked at 400 nm has to be ascribed to the formation of the closed-shell compounds **8-oxoA** (Tables S21 and S22), which clearly absorb at much shorter wavelengths. In addition, protonation of the 8-oxygenated intermediates expected at acid conditions (**A8OHH**$^{+}$, **A8N9H**$^{+}$, and **A8FORMH**$^{+}$) does not significantly shift the absorption spectra of the radicals (see Tables S29−S31). Moreover, oxidation kinetics of **A8OHH**$^{+}$ and **A8FORMH**$^{+}$ are similar, whereas the $\Delta G_{ET}^{\ddagger}$ value for **A8N9H**$^{+}$ is clearly larger than that of the former two compounds (see Table 2).

The **A8OH**/**A8N9**/**A8FORM** distribution is expected to change at acid pH since the ring-opened radicals **A8N9** and **A8FORM** are expected to be more accessible with respect to neutral conditions. The cause is that at low pH the reaction mechanism presented in Scheme 2 can be efficiently catalyzed by the presence of H^+. The **A8OH** transformation to **A8ZW** requires protonation at the N7 site (see Figure S25) where the proton donor is a water molecule at neutral pH. It is therefore reasonable to expect that acid pH will significantly accelerate this process since H^+ (or H_3O^+) is a much more efficient proton donor, increasing the production of **A8ZW** radical and ultimately the yield of **A8N9** and **A8FORM** compounds.

It is worth mentioning that the oxidation mechanisms ($-e^-$, $-H^+$) of **A8OH** and **A8N9**/**A8FORM** are not equal since the main final oxidation products (**8-oxoAoh** and **8-oxoAco**) are closed-ring structures, while **A8N9**/**A8FORM** are opened-ring compounds. This suggests that the opened-ring radicals **A8N9** and **A8FORM** *must* undergo an endergonic ring-closure process to ultimately yield the **8-oxoA** species. Indeed, deprotonation of the oxidized **A8FORM**$^{+}$ species (see structure at Table S25) from the C8 position does not open any chemical pathway to produce **8-oxoA**. Thus, **A8FORM**/**A8FORMH**$^{+}$ species have to be necessarily converted to the more energetic

DOI: 10.1021/acs.joc.6b02393
J. Org. Chem. 2017, 82, 276−288

Table 3. Comparison of the Gibbs Activation Energies (kcal/mol) and Kinetic Constants (s^{-1}) Computed for the Most Important A + •OH Addition Channels[a]

method	•OH addition channel				
	C2	C4	C5	C8	C5/C8 rate constants ratio
			$\Delta G^{\ddagger}$		
ωB97X-D[b]	12.66	13.41	10.20	5.60	
ωB97X-D-(PCM/Explicit)[c]	12.65	14.93	12.00	8.82	
M06-2X[d]	14.66	14.54	11.40	7.56	
CCSD(T)//M06-2X[d,e]	15.49	14.82	11.43	8.80	
M06-2X-(PCM)[d]	14.76	15.77	10.82	9.96	
CCSD(T)-(PCM)//M06-2X-(PCM)[d,f]	15.24	15.62	10.49	10.72	
			k (298.15 K)		
CCSD(T)//M06-2X[d,e]	5.48×10^{1}	1.70×10^{2}	5.19×10^{4}	4.40×10^{6}	0.01
CCSD(T)-(PCM)//M06-2X-(PCM)[d,f]	8.36×10^{1}	$4{,}40 \times 10^{1}$	$2{,}54 \times 10^{5}$	$1{,}72 \times 10^{5}$	1.48
			Experimental Yield (%) (pH ~ 7)[g]		
				~18	

[a]Experimental determinations are also shown. [b]6-311++G(2df,2dp) basis set, taken from ref 34. [c]6-311++G(2df,2dp) basis set including one explicit water molecule and PCM method, taken from ref 35. [d]6-31++G(d,p) basis set, present work. [e]Zero-point vibrational, thermal, and entropy contributions to energy computed at the M06-2X/6-31++G(d,p) level. [f]Zero-point vibrational, thermal, and entropy contributions to energy computed at the M06-2X-(PCM)/6-31++G(d,p) level. [g]Data from product analysis in ref 16.

A8N9/A8N9H$^+$ radicals, which have H atoms at both N7 and N9 positions. The mentioned **A8FORMH$^+$** → **A8N9H$^+$** transformation has a barrier of $\Delta G^{\ddagger}$ = 13.23 kcal/mol (see Scheme S4), which is similar to the value of $\Delta G^{\ddagger}$ = 14.15 kcal/mol computed for the neutral **A8FORM** → **A8N9** reaction (see Scheme 4 and Figure 3). Later, dehydrogenation from the C8 position can trigger the ring-closure process leading to **8-oxoAco** or its protonated analogue. Conversely, **A8OH/A8OHH$^+$** oxidation does not require a ring-closure reaction, and deprotonation of **A8OH$^+$/A8OHH^{2+}** (see structure in Table S25) from the C8 position directly produces **8oxoAoh** or its protonated species. For this reason, and also taking into account the slower electron-transfer reaction computed for **A8N9/A8N9H$^+$** (more accessible at acid pH), it becomes apparent that the closed-ring radicals are easily oxidized as compared to the opened-ring tautomers. The reaction mechanism proposed in this work supports a significant acid catalysis of the **A8OH** → **A8ZW** transformation, increasing therefore the abundance of **A8N9** and **A8FORM** radicals in the reaction medium at low pH. The slower oxidation of the latter compounds is responsible of the *decrease* of the total oxidation rate tracked at ~400 nm.

Finally, the acid catalysis of the ring-opening processes of **A8OH** correlates well with the product analysis of the **8-oxoAoh** yield as a function of pH, data reported by Vieira and Steenken[16] and reproduced in Figure 4b (plot in squares). The yield of **8-oxoAoh** product drops from ~18% at neutral pH to ~5% at pH = 3. It can be rationalized by taking into account the larger ratio of ring-opened radicals **A8N9** and **A8FORM** with respect to the ring-closed **A8OH** system, decreasing the formation of **8-oxoAoh** and favoring other disappearance processes.

Revision of the Yield of OH Radical Addition to Adenine. Determination of the relative yields of the three competitive mechanisms in the •OH reaction with NBs, namely addition to double bonds, H atom abstraction, and one-electron reactions is challenging because requires accurate calculations of electron transfer rates, TS structures, and tunneling effects. The yield of addition reactions is estimated on the basis of accurate TS computations carried out in this work and using the ~18% of addition to C8 position determined by product analysis[16] as a reference. Table 3 summarizes the Gibbs activation barriers obtained with different methods for the •OH addition to C2, C4, C5, and C8 positions (atom numbering displayed in Figure 1a). Previous calculations in vacuo with the ωB97X-D functional,[34] which are in agreement with the present M06-2X and CCSD(T) results without the use of the PCM method, suggested that addition to the C8 position is the most favorable channel. Nevertheless, when solvent effects are included in the model, the C5 and the C8 pathways become almost degenerate and therefore competitive. Solvation can be estimated by the analysis of the dipole moment modules ($|\vec{\mu}|$) of the TSs for the C4, C5, and C8 addition, which are 3.88, 5.88, and 3.18 D, respectively. Thus, solvent effects are expected to stabilize to a greater extent the TS related to the addition to the C5 atom. On the other hand, explicit solvation of the TS with six water molecules inverts the trend and establishes the C5 channel as the preferred pathway, as the C8 and the C4 TSs are 4.97 and 1.32 kcal/mol higher in energy, respectively. Therefore, it can be concluded that the TSs for both C5 and C8 channels are quasi-degenerated in water solution, and both pathways have to be considered competitive. This behavior is not observed with the ωB97X-D functional accounting solvent effects by means of PCM and/or explicit water molecules.[35]

In order to estimate the C5 reaction yield, kinetic constants have been calculated using the conventional transition-state theory (eq 7)[81,82]

$$k = \sigma \frac{k_B T}{h} e^{(-\Delta G^{\ddagger}/RT)} \quad (7)$$

where σ states for the symmetry factor (two for the addition reactions); k_B, h, and R stand for the Boltzmann, Planck, and gas constants, respectively; and $\Delta G^{\ddagger}$ refers to the Gibbs activation energy computed at the CCSD(T)-(PCM)//M06-2X-(PCM) level. Results are compiled in Table 3. It can be readily seen that the ~5 kcal/mol energy difference of the TS corresponding to the C4 addition in solution has a strong impact on the rate constant, being 5 orders of magnitude smaller than that of C5 and C8 channels. Using the experimental determination of the addition yield to the C8 position (~18%),[16] a percentage of ~26.5% is estimated for the

DOI: 10.1021/acs.joc.6b02393
J. Org. Chem. 2017, 82, 276−288

C5 pathway since the ratio of the C5/C8 rate constants is 1.47. Thus, the sum of the two channels gives rise to, at least, a ∼44.5% of total •OH addition to **A** in water solution. On the other hand, C4 and C2 routes can be safely considered minor paths. The remaining ∼55.5% is therefore ascribed to H atom abstraction[33,34] and one-electron reaction (eq 1) mechanisms. Both processes produce **ANH** radical, which is expected to be repaired to **A** via oxidation of **A8OH**. It is important to remark that this estimation is compatible with the important role of the H atom abstraction reactions recently reported by Milhøj and Sauer[34,68] and Chatgilialoglu et al.[74,83] for purine nucleobases.

Comments on the •OH Addition to Adenine within the Biological DNA Environment. The understanding of the •OH addition to **A** in the gas phase and water solution carried out in this contribution allow us to make some useful considerations regarding the regioselectivity and efficiency of the reaction in biological DNA/RNA structures. Two main aspects determine the rate of the addition reaction: (i) the accessibility of the NB and each atomic position to the OH radical and (ii) the intrinsic reactivity of each position, which can depend on the interaction with water or other surrounding structures. The current research sheds light on the latter issue and the solvent effects. It has been proposed that solvent accessibility in the microenvironment of nucleic acids is somewhat restricted due to the hydrophobic character of the double strand and, among other factors, the presence of DNA−protein complexes,[26] suggesting that DNA/RNA macromolecules should not be considered completely solvated. Actually, a recent measurement of the dielectric constant of DNA yielded a value of ∼8,[84] which is ca. 1 order of magnitude smaller than that of water. For this reason, •OH additions in vivo should behave somehow between the descriptions provided in vacuo and the completely solvated environment using the PCM method and explicit water molecules. The following specific considerations emerge from the present work: (i) solvation of the NB surroundings *increases* the C5 addition rate due to a significant stabilization of the TS, raising the C5/C8 ratio (see Table 3) and, consequently, promotes the formation of electron holes ($\mathbf{A}^{\bullet+}$, see Scheme 1) along the DNA/RNA structure; (ii) a more efficient solvation slightly decreases the C8 addition rate, as demonstrated by the comparison between the Gibbs activation barriers in vacuo and in solution (Table 3), and consequently hampers the formation of **8-oxoA** and **FAPyA** mutagens, but favors their production with respect to electron holes ($\mathbf{A}^{\bullet+}$), and (iii) ring-opening reactions of **A8OH** in hydrophobic environments are expected to be slower as compared to full solvated conditions, since water molecules actively catalyze the chemical transformations.

CONCLUSIONS

In the present contribution, the reaction mechanisms of the •OH addition to adenine have been studied by means of DFT/M06-2X, CCSD(T), and CASPT2//CASSCF calculations. The experimental data[16−18] used as a reference in the last 30 years have been reinterpreted on the basis of the Gibbs activation barriers, thermodynamics, and vertical absorption energies of the radical intermediates derived from the •OH reaction with adenine.

The present theoretical results confirm that addition of the OH radical to adenine in water solution gives rise almost exclusively to the radicals **A5OH** and **A8OH**. The latter species undergo ring-opening reactions followed by oxidation/reduction of the intermediates to produce the **8-oxoA** and **FAPyA** mutagens. The detailed mechanisms of the ring-opening processes are reported, demonstrating that **A8OH** is transformed to the formamidopyridine radical **A8FORM** on a miscrosecond scale. Two more intermediates, namely **A8ZW** and **A8N9**, partake in the process. Analysis of the spectroscopic features of the radicals indicates that the 8-oxygenated radicals **A8OH**, **A8N9**, and **A8FORM** absorb in the ∼400 nm region. This assignation establishes a new scenario of the spectroscopy of the adenine + •OH reaction. It is concluded that the optical density time decay of the signal at ∼400 nm observed experimentally from 2 to 30 μs[16] is caused by the oxidation or reduction of the **A8OH**, **A8N9**, and **A8FORM** radical intermediates. On the other hand, optical changes at ∼330 are assigned to the formation of the dehydrogenated adenine radical **ANH**, which is the result of the dehydration of **A5OH**. The assignations are consistent with the reported O_2 quenching rates,[16] which have been reinterpreted on the basis of M06-2X-(PCM) energy barriers, and the pH dependencies of the optical changes at ∼400 and ∼330 nm.

Finally, in contrast to previous interpretations, addition to the C4 position is of minor importance in light of the high-energy TS determined for the process and the re-evaluation of the experimental recordings. By combining the reaction rates computed in the present work and product analysis data documented by Vieira and Steenken,[16] the total yield of •OH addition to adenine is estimated to be, at least, ∼44.5% in water solution. The present results are important in the understanding of the adenine oxidation in the DNA environment, where the solvation is expected to be less efficient than in water solution. It is predicted that, for the •OH reaction with adenine in real DNA/RNA environments, addition to the C8 position will be the preferred addition channel, having a total adducts distribution somewhere in between the gas-phase and the water-solvated results. Accordingly, higher yields of the **8-oxoA** and **FAPyA** mutagens are expected in living cells with respect to fully solvated nucleobases in water.

ASSOCIATED CONTENT

Supporting Information

The Supporting Information is available free of charge on the ACS Publications website at DOI: 10.1021/acs.joc.6b02393.

Calibration of M06-2X energies; details on the SA-CASSCF/CASPT2 calculations; vertical absorption energies, oscillator strengths, and dipole moment modules of the excited states; reaction barriers of the studied compounds with O_2; energetics of the solvation of the TS corresponding to the •OH addition to C4 and C5; λ reorganization energies; analysis of secondary pathways; and Cartesian coordinates of the studied species (PDF)

AUTHOR INFORMATION

Corresponding Authors

*E-mail: antonio.frances@uv.es.
*E-mail: daniel.roca@uv.es.

ORCID

Antonio Francés-Monerris: 0000-0001-8232-4989

Notes

The authors declare no competing financial interest.

DOI: 10.1021/acs.joc.6b02393
J. Org. Chem. 2017, 82, 276−288

■ ACKNOWLEDGMENTS

We are grateful to Josep Vicent Borràs de Llano and Franziska Schüppel for help with some of the calculations and to Dr. Juan Aragó for the fruitful discussions about electron-transfer reactions. This work has been funded by Ministerio de Economía y Competitividad (project CTQ2014-58624-P and "Juan de la Cierva" contract JCI-2012-13431).

■ REFERENCES

(1) Kadlec, A. O.; Beyer, A. M.; Ait-Aissa, K.; Gutterman, D. D. *Basic Res. Cardiol.* **2016**, *111*, 12.
(2) Maiolino, G.; Azzolini, M.; Rossi, G. P.; Davis, P. A.; Calo, L. A. *Free Radical Biol. Med.* **2015**, *88*, 51−58.
(3) Rochette, L.; Zeller, M.; Cottin, Y.; Vergely, C. *Biochim. Biophys. Acta, Gen. Subj.* **2014**, *1840*, 2709−2729.
(4) Kowluru, R. A.; Mishra, M. *Biochim. Biophys. Acta, Mol. Basis Dis.* **2015**, *1852*, 2474−2483.
(5) Tulah, A. S.; Birch-Machin, M. A. *Mitochondrion* **2013**, *13*, 444−453.
(6) Payne, B. A. I.; Chinnery, P. F. *Biochim. Biophys. Acta, Bioenerg.* **2015**, *1847*, 1347−1353.
(7) Wen, X.; Wu, J.; Wang, F.; Liu, B.; Huang, C.; Wei, Y. *Free Radical Biol. Med.* **2013**, *65*, 402−410.
(8) Lepetsos, P.; Papavassiliou, A. G. *Biochim. Biophys. Acta, Mol. Basis Dis.* **2016**, *1862*, 576−591.
(9) Cadet, J.; Douki, T.; Ravanat, J.-L. *Photochem. Photobiol.* **2015**, *91*, 140−155.
(10) Dantas, A. D.; Day, A.; Ikeh, M.; Kos, I.; Achan, B.; Quinn, J. *Biomolecules* **2015**, *5* (1), 142−165.
(11) Kim, K. E.; Cho, D.; Park, H. J. *Life Sci.* **2016**, *152*, 126−134.
(12) Breen, A. P.; Murphy, J. A. *Free Radical Biol. Med.* **1995**, *18*, 1033−1077.
(13) Dizdaroglu, M. *Mutat. Res., Rev. Mutat. Res.* **2015**, *763*, 212−245.
(14) *The Nobel Prize in Chemistry 2015*; Nobel Media AB, 2014. Web. 28 Jul 2016, http://www.nobelprize.org/nobel_prizes/chemistry/laureates/2015/ (accessed 28 Jul 2016).
(15) von Sonntag, C. *Free-Radical-Induced DNA Damage and Its Repair: A Chemical Perspective*; Springer-Verlag: Berlin, 2006.
(16) Vieira, A.; Steenken, S. *J. Am. Chem. Soc.* **1990**, *112*, 6986−6994.
(17) Vieira, A.; Steenken, S. *J. Phys. Chem.* **1987**, *91*, 4138−4144.
(18) Vieira, A.; Steenken, S. *J. Am. Chem. Soc.* **1987**, *109*, 7441−7448.
(19) Candeias, L. P.; Steenken, S. *Chem. - Eur. J.* **2000**, *6*, 475−484.
(20) Schuchmann, M. N.; Steenken, S.; Wroblewski, J.; von Sonntag, C. *Int. J. Radiat. Biol. Relat. Stud. Phys., Chem. Med.* **1984**, *46*, 225−232.
(21) Hayon, E.; Simic, M. *J. Am. Chem. Soc.* **1973**, *95*, 1029−1035.
(22) Blok, J.; Loman, H. *Curr. Top. Radiat. Res. Q.* **1973**, *9*, 165.
(23) Scholes, G. *Annu. Rep. Prog. Chem., Sect. A: Gen., Phys. Inorg. Chem.* **1970**, *67*, 169.
(24) Van Hemmen, J. J. *Int. J. Radiat. Biol. Relat. Stud. Phys., Chem. Med.* **1975**, *27*, 403−407.
(25) O'Neill, P.; Chapman, P. W.; Papworth, D. G. *Free Radicals in Biology and Medicine*; Harwood: Chur, 1985; p 62.
(26) Aparici-Espert, I.; Francés-Monerris, A.; Rodríguez-Muñiz, G. M.; Roca-Sanjuán, D.; Lhiaubet-Vallet, V.; Miranda, M. A. *J. Org. Chem.* **2016**, *81*, 4031−4038.
(27) Kobayashi, K. *J. Phys. Chem. B* **2010**, *114*, 5600−5604.
(28) Banyasz, A.; Ketola, T.-M.; Muñoz-Losa, A.; Rishi, S.; Adhikary, A.; Sevilla, M. D.; Martínez-Fernández, L.; Improta, R.; Markovitsi, D. *J. Phys. Chem. Lett.* **2016**, *7*, 3949−3953.
(29) Adhikary, A.; Becker, D.; Collins, S.; Koppen, J.; Sevilla, M. D. *Nucleic Acids Res.* **2006**, *34*, 1501−1511.
(30) Candeias, L. P.; Steenken, S. *J. Am. Chem. Soc.* **1993**, *115*, 2437−2440.
(31) Oneill, P.; Davies, S. E. *Int. J. Radiat. Biol.* **1987**, *52*, 577−587.
(32) Ito, T.; Kuno, S.; Uchida, T.; Fujita, S.-i.; Nishimoto, S.-i. *J. Phys. Chem. B* **2009**, *113*, 389−394.
(33) Cheng, Q. Y.; Gu, J. D.; Compaan, K. R.; Schaefer, H. F. *Chem. - Eur. J.* **2010**, *16*, 11848−11858.
(34) Milhøj, B. O.; Sauer, S. P. A. *J. Phys. Chem. A* **2015**, *119*, 6516−6527.
(35) Milhøj, B.; Sauer, S. P. A. *ChemPhysChem* **2016**, *17*, 3086−3095.
(36) Naumov, S.; von Sonntag, C. *Radiat. Res.* **2008**, *169*, 355−363.
(37) Munk, B. H.; Burrows, C. J.; Schlegel, H. B. *Chem. Res. Toxicol.* **2007**, *20*, 432−444.
(38) Kumar, A.; Pottiboyina, V.; Sevilla, M. D. *J. Phys. Chem. B* **2011**, *115*, 15129−15137.
(39) Liao, X. F.; Diao, L.; Kou, L.; Li, Z. G.; Li, M. J.; Lu, W. C. *J. Phys. Org. Chem.* **2015**, *28*, 645−651.
(40) Kamiya, H.; Miura, H.; Muratakamiya, N.; Ishikawa, H.; Sakaguchi, T.; Inoue, H.; Sasaki, T.; Masutani, C.; Hanaoka, F.; Nishimura, S.; Ohtsuka, E. *Nucleic Acids Res.* **1995**, *23*, 2893−2899.
(41) Talhaoui, I.; Couve, S.; Ishchenko, A. A.; Kunz, C.; Schar, P.; Saparbaev, M. *Nucleic Acids Res.* **2013**, *41*, 912−923.
(42) Dizdaroglu, M.; Kirkali, G.; Jaruga, P. *Free Radical Biol. Med.* **2008**, *45*, 1610−1621.
(43) Zhao, Y.; Truhlar, D. G. *Theor. Chem. Acc.* **2008**, *120* (1−3), 215−241.
(44) *Gaussian 09*, revision D.01: Frisch, M. J.; Trucks, G. W.; Schlegel, H. B.; Scuseria, G. E.; Robb, M. A.; Cheeseman, J. R.; Scalmani, G.; Barone, V.; Mennucci, B.; Petersson, G. A.; Nakatsuji, H.; Caricato, M.; Li, X.; Hratchian, H. P.; Izmaylov, A. F.; Bloino, J.; Zheng, G.; Sonnenberg, J. L.; Hada, M.; Ehara, M.; Toyota, K.; Fukuda, R.; Hasegawa, J.; Ishida, M.; Nakajima, T.; Honda, Y.; Kitao, O.; Nakai, H.; Vreven, T.; Montgomery, J. A., Jr.; Peralta, J. E.; Ogliaro, F.; Bearpark, M.; Heyd, J. J.; Brothers, E.; Kudin, K. N.; Staroverov, V. N.; Kobayashi, R.; Normand, J.; Raghavachari, K.; Rendell, A.; Burant, J. C.; Iyengar, S. S.; Tomasi, J.; Cossi, M.; Rega, N.; Millam, J. M.; Klene, M.; Knox, J. E.; Cross, J. B.; Bakken, V.; Adamo, C.; Jaramillo, J.; Gomperts, R.; Stratmann, R. E.; Yazyev, O.; Austin, A. J.; Cammi, R.; Pomelli, C.; Ochterski, J. W.; Martin, R. L.; Morokuma, K.; Zakrzewski, V. G.; Voth, G. A.; Salvador, P.; Dannenberg, J. J.; Dapprich, S.; Daniels, A. D.; Farkas, Ö.; Foresman, J. B.; Ortiz, J. V.; Cioslowski, J.; Fox, D. J. Gaussian, Inc., Wallingford, CT, 2013.
(45) Mardirossian, N.; Head-Gordon, M. *J. Chem. Theory Comput.* **2016**, *12*, 4303−25.
(46) Xu, X.; Alecu, I. M.; Truhlar, D. G. *J. Chem. Theory Comput.* **2011**, *7*, 1667−1676.
(47) Isayev, O.; Gorb, L.; Leszczynski, J. *J. Comput. Chem.* **2007**, *28*, 1598−1609.
(48) Francés-Monerris, A.; Merchán, M.; Roca-Sanjuán, D. *J. Phys. Chem. B* **2014**, *118*, 2932−2939.
(49) Galano, A.; Alvarez-Idaboy, J. R. *Org. Lett.* **2009**, *11*, 5114−5117.
(50) Liptak, M. D.; Shields, G. C. *J. Am. Chem. Soc.* **2001**, *123*, 7314−7319.
(51) Thapa, B.; Schlegel, H. B. *J. Phys. Chem. A* **2015**, *119*, 5134−5144.
(52) Palascak, M. W.; Shields, G. C. *J. Phys. Chem. A* **2004**, *108*, 3692−3694.
(53) Camaioni, D. M.; Schwerdtfeger, C. A. *J. Phys. Chem. A* **2005**, *109*, 10795−10797.
(54) Kelly, C. P.; Cramer, C. J.; Truhlar, D. G. *J. Phys. Chem. B* **2006**, *110*, 16066−16081.
(55) Schmid, R.; Miah, A. M.; Sapunov, V. N. *Phys. Chem. Chem. Phys.* **2000**, *2*, 97−102.
(56) Autrey, T.; Brown, A. K.; Camaioni, D. M.; Dupuis, M.; Foster, N. S.; Getty, A. *J. Am. Chem. Soc.* **2004**, *126*, 3680−3681.
(57) Giussani, A.; Segarra-Martí, J.; Roca-Sanjuán, D.; Merchán, M. *Top. Curr. Chem.* **2013**, *355*, 57−97.
(58) Roca-Sanjuán, D.; Fdez. Galván, I.; Lindh, R.; Ya-Jun, L. Recent Method Developments and Applications in Computational Photochemistry, Chemiluminescene and Bioluminescence. In *Photochemistry*; Fasani, E., Albini, A., Eds.; RSC: London, 2015; Vol. *42*, pp 11−42.
(59) Roca-Sanjuán, D.; Aquilante, F.; Lindh, R. *Wiley Interdiscip. Rev.: Comput. Mol. Sci.* **2012**, *2*, 585−603.

DOI: 10.1021/acs.joc.6b02393
J. Org. Chem. 2017, 82, 276−288

(60) Serrano-Pérez, J. J.; Serrano-Andrés, L., Calculation of Excited States: Molecular Photophysics and Photochemistry on Display. In *Handbook of Computational Chemistry*; Leszczynski, J., Ed.; Springer-Verlag: Berlin, 2012; pp 483−560.
(61) Roos, B. O.; Andersson, K.; Fulscher, M. P.; Malmqvist, P. Å.; Serrano-Andrés, L.; Pierloot, K.; Merchán, M. Multiconfigurational Perturbation Theory: Applications in Electronic Spectroscopy. In *Advances in Chemical Physics: New Methods in Computational Quantum Mechanics*; Prigogine, I., Rice, S. A., Eds.; John Wiley & Sons, Inc.: Hoboken, NJ, 2007; Vol. *93*, pp 219−331.
(62) Malmqvist, P. Å.; Rendell, A.; Roos, B. O. *J. Phys. Chem.* **1990**, *94*, 5477−5482.
(63) Andersson, K.; Malmqvist, P. Å.; Roos, B. O.; Sadlej, A. J.; Wolinski, K. *J. Phys. Chem.* **1990**, *94*, 5483−5488.
(64) Andersson, K.; Malmqvist, P. Å.; Roos, B. O. *J. Chem. Phys.* **1992**, *96*, 1218−1226.
(65) Widmark, P. O.; Malmqvist, P. Å.; Roos, B. O. *Theor. Chim. Acta* **1990**, *77*, 291−306.
(66) Francés-Monerris, A.; Merchán, M.; Roca-Sanjuán, D. *J. Chem. Phys.* **2013**, *139*, 071101.
(67) Aquilante, F.; Autschbach, J.; Carlson, R. K.; Chibotaru, L. F.; Delcey, M. G.; De Vico, L.; Galvan, I. F.; Ferre, N.; Frutos, L. M.; Gagliardi, L.; Garavelli, M.; Giussani, A.; Hoyer, C. E.; Li Manni, G.; Lischka, H.; Ma, D.; Malmqvist, P. Å.; Mueller, T.; Nenov, A.; Olivucci, M.; Pedersen, T. B.; Peng, D.; Plasser, F.; Pritchard, B.; Reiher, M.; Rivalta, I.; Schapiro, I.; Segarra-Marti, J.; Stenrup, M.; Truhlar, D. G.; Ungur, L.; Valentini, A.; Vancoillie, S.; Veryazov, V.; Vysotskiy, V. P.; Weingart, O.; Zapata, F.; Lindh, R. *J. Comput. Chem.* **2016**, *37*, 506−541.
(68) Milhøj, B. O.; Sauer, S. P. A. *Chem. - Eur. J.* **2015**, *21*, 17786−17799.
(69) Fukuzumi, S.; Miyao, H.; Ohkubo, K.; Suenobu, T. *J. Phys. Chem. A* **2005**, *109*, 3285−3294.
(70) Kittler, L.; Lober, G.; Gollmick, F. A.; Berg, H. *Bioelectrochem. Bioenerg.* **1980**, *7*, 503−511.
(71) Schwarz, H. A.; Dodson, R. W. *J. Phys. Chem.* **1984**, *88*, 3643−3647.
(72) Steenken, S. *Chem. Rev.* **1989**, *89*, 503−520.
(73) Llano, J.; Eriksson, L. A. *Phys. Chem. Chem. Phys.* **2004**, *6*, 2426−2433.
(74) Chatgilialoglu, C.; D'Angelantonio, M.; Kciuk, G.; Bobrowski, K. *Chem. Res. Toxicol.* **2011**, *24*, 2200−2206.
(75) Greenberg, M. M. *Acc. Chem. Res.* **2012**, *45*, 588−597.
(76) Kalam, M. A.; Haraguchi, K.; Chandani, S.; Loechler, E. L.; Moriya, M.; Greenberg, M. M.; Basu, A. K. *Nucleic Acids Res.* **2006**, *34*, 2305−2315.
(77) Senturker, S.; Dizdaroglu, M. *Free Radical Biol. Med.* **1999**, *27*, 370−380.
(78) Poskrebyshev, G. A.; Neta, P.; Huie, R. E. *J. Phys. Chem. A* **2002**, *106*, 11488−11491.
(79) Scholes, M. L.; Schuchmann, M. N.; von Sonntag, C. *Int. J. Radiat. Biol.* **1992**, *61*, 443−449.
(80) Marcus, R. A. *Rev. Mod. Phys.* **1993**, *65*, 599−610.
(81) Eyring, H. *J. Chem. Phys.* **1935**, *3*, 107−115.
(82) Truhlar, D. G.; Garrett, B. C.; Klippenstein, S. J. *J. Phys. Chem.* **1996**, *100*, 12771−12800.
(83) Chatgilialoglu, C.; D'Angelantonio, M.; Guerra, M.; Kaloudis, P.; Mulazzani, Q. G. *Angew. Chem., Int. Ed.* **2009**, *48*, 2214−2217.
(84) Cuervo, A.; Dans, P. D.; Carrascosa, J. L.; Orozco, M.; Gomila, G.; Fumagalli, L. *Proc. Natl. Acad. Sci. U. S. A.* **2014**, *111*, E3624−E3630.

DOI: 10.1021/acs.joc.6b02393
J. Org. Chem. 2017, 82, 276−288